A Novel Compact Reconfigurable Broadband Antenna for Cognitive Radio Applications

Adnan Kantemur, Jinpil Tak, *Member, IEEE*, Peyman Siyari, Ahmed H. Abdelrahman, *Senior Member, IEEE,* Marwan Krunz, *Fellow, IEEE* and Hao Xin, *Fellow, IEEE*

***Abstract*—A novel reconfigurable antenna covering an 11.5:1 bandwidth is designed and fabricated for cognitive radio applications. The proposed novel antenna has two independent paths to cover 430 MHz to 5 GHz frequency range. The first path is directly connected to an ultra-wide-band antenna, which covers 1–5 GHz operation frequency range. The second path, for the frequency range between 430 MHz and 1 GHz, goes through a dc-controlled varactor based matching network. The switching functionality between wideband (1 to 5 GHz) and reconfigurable region (430 MHz to 1 GHz) is realized by two discrete switches. The designed antenna has a simple structure and compact size of 60 mm × 100 mm. The proposed novel antenna has great potential for use in cognitive radio systems.**

***Index Terms*— reconfigurable antenna; UWB; cognitive radio.**

I. Introduction

Massive data traffic and high data rate are very critical issues in modern communication. Today there are more than 400 million wireless subscribers in the USA, equal to 1.2 wireless devices for every person in the country and wireless data traffic increased by nearly four times between 2014 and 2017 [1]. The ever-growing data demand creates a shortage in the wireless spectrum. Besides this well-known spectrum shortage, spectrum usage is not uniformly distributed which leads to inefficiency. In order to overcome spectrum crowdedness and address inefficient spectrum usage, cognitive radio systems that are aware of unoccupied and/or idle state frequency bands and then adaptively change its operation to establish a reliable communication are required. Wideband antennas that can operate at any spectrum are very attractive for cognitive radio systems. In addition, compact antenna size is demanded to be suitable for portable and mobile devices.

Most of the antennas currently used in wireless systems such as cellular network are classified as "resonant" antennas and intrinsically narrow band, for example, they can only operate at a fixed frequency with a small fractional bandwidth ranging from ~ 3% (for patch antennas) to ~ 10% (for dipole antennas). Thus, they are not suitable for realizing a robust cognitive radio whose operating frequency needs to hop over multiple octaves of the frequency range.

Broader band antennas exist that can operate over a large bandwidth, for example, log-periodic antennas, horn antennas, etc. However, they belong to the other antenna class – "traveling wave" antennas, and are much larger in size (i.e., with electrical size several wavelengths or more) compared to "resonant" antennas (usually smaller than unit wavelength). For example, a broadband double-ridged horn antenna (AINFO-LB-460) that can operate from 400 MHz to 6 GHz has a dimension of 49.2 cm × 32.2 cm × 43.6 cm. On the other hand, Choi *et al.* [2] introduced printed UWB monopole antennas and they became popular for mobile wireless device applications. The printed UWB monopole antenna consists of a monopole patch and a partial ground plane. Various geometries (rectangular, circular, elliptical, triangular, hexagonal, etc.) of the monopole patch have been implemented to achieve UWB behavior [3-8]. The most commonly used definition for the UWB antennas is the bandwidth ratio (high frequency to low frequency ratio) [9],[10] and typically, these antennas can achieve an impedance bandwidth ratio up to 4:1.

In recent years, reconfigurable antennas based on various tuning mechanisms including semiconductor varactors [11-14], PIN diodes [15-18], micro-electro-mechanical system (MEMS) devices [19-21], ferrites [22-25], and liquid crystals [26-29] have been extensively studied. Being able to dynamically cover multiple frequency bands and provide multiple functionalities, these reconfigurable antennas have the potential benefits of reducing system cost and enable the desired dynamic spectrum access. However, due to limitations such as finite tuning range and associated losses, it is still difficult to obtain a reconfigurable antenna with large enough frequency tuning range demanded by cognitive radio systems. There are two types of tuning approach to realize reconfigurable circuits/antennas, namely, switching type and continuous tuning type. For the former, switches (e.g., MEMS or PIN diode based) are used to obtain digital tuning, for example, toggling between two discrete frequency bands. In [18] and [19], microstrip patch antennas operating at 1.33 and 2.95 GHz and 1.5 and 9.6 GHz, respectively, were reported. This approach allows relatively large difference for the discrete bands but is not suitable for the proposed cognitive radio that needs to cover a large number of frequency bands. For the latter, continuously tunable devices/materials (e.g., varactors, ferroelectric materials, ferromagnetic materials, and liquid crystals) are utilized to realize continuous tuning in an analog fashion. However, the tuning range is often limited. For example, in [11], a varactor-loaded patch antenna was reported to operate in a single narrow channel tunable from 890 to 1500 MHz; in [29], a liquid-crystal tuned patch antenna operating at 5 GHz achieved a 4 – 8% tuning range; in [23], a ferroelectric material tuned slot antenna was reported to have continuous narrow band tuning from 6.71 to 9.14 GHz; in [24], a magnetically tunable ferrite loaded waveguide antenna obtained continuous narrow band tuning from 9.95 to 11.06 GHz. In summary, most of the reported reconfigurable antennas have limited frequency tuning range (i.e., less than 2:1 ratio for center frequency) which is not adequate for a robust cognitive radio system that may need to have a 10:1 center frequency tuning ratio.

Manuscript received May 9, 2019. This work was supported in part by the U.S. National Science Foundation under Grant 1513649.

Adnan Kantemur, Jinpil Tak, Peyman Siyari, Merwan Krunz, and Hao Xin are with the University of Arizona, Tucson, AZ 85721 USA ({akantemur; abrahamtak; psiyari; krunz; hxin} @ email.arizona.edu).

Ahmed H. Abdelrahman was with the University of Arizona, Tucson, AZ 85721 USA, and he is currently with Analog Devices Inc., Greensboro, NC 27409 USA (ahmed.h.abdelrahman@ieee.org)

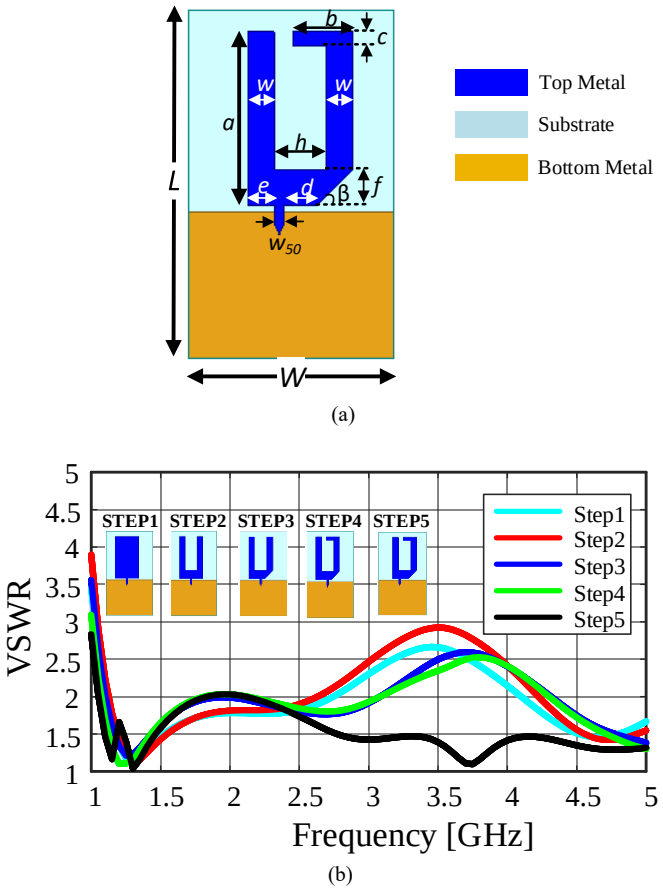

Fig. 1. Proposed antenna: (a) Geometry of the UWB Antenna: L=100mm, W=60mm, a=50mm, b=17mm, c=4mm, d=9.8mm, e=7.8mm, f=10mm, β=45^0, g=42.2mm, h=15mm, w=7.5mm, w_{50} =2.4mm; (b) Design procedure of the UWB Antenna

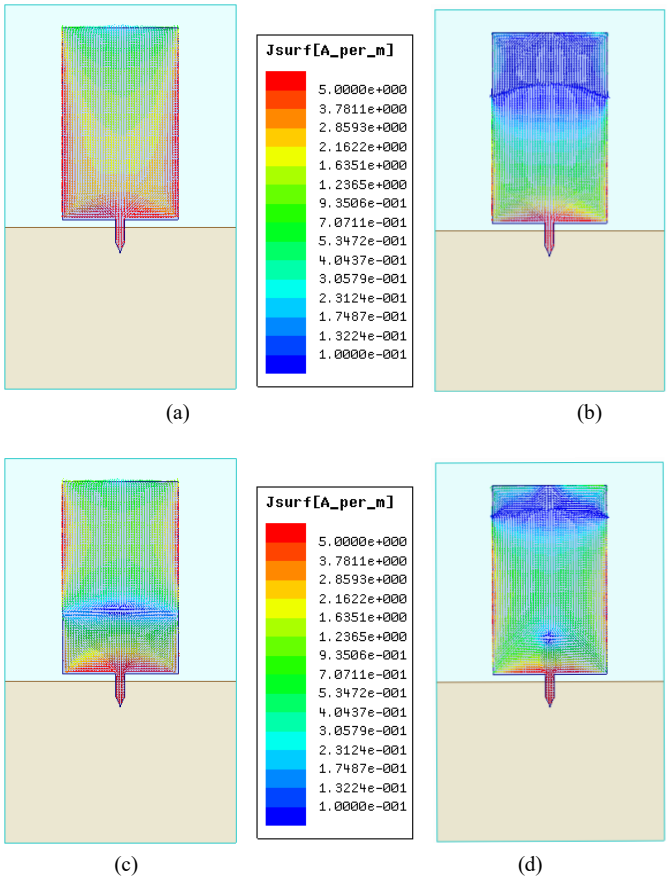

Fig. 2. Surface current distribution of the initial UWB antenna at various frequencies: (a) 1 GHz; (b) 2 GHz; (c) 3 GHz; (d) 4 GHz

In this paper, a novel reconfigurable broadband antenna that can operate in a wide frequency range (BW ratio ≥ 10:1) while having compact size so that it is suitable for portable devices is proposed. Both the discrete switching and continuously tuning techniques are used to obtain the proposed large frequency coverage. The proposed antenna features a UWB monopole configuration combined with a tunable matching network. The antenna has two independent paths to cover 430 MHz to 5 GHz frequency range. The first path is directly connected to the UWB antenna, which covers 1–5 GHz operation frequency range. The second path, for the frequency range between 430 MHz and 1 GHz, goes through a dc-controlled varactor based matching network, which matches the UWB antenna. An additional switch is used to connect both paths to achieve a single input/output configuration. The switching functionality between the wideband and reconfigurable region is realized by two discrete switches. This unique combination of switches and the varactor provides an extremely wide (11.5:1) frequency operation region. The designed antenna has a simple structure and compact size of 60 mm × 100 mm which is suitable for mobile wireless devices. Note that size of a typical smartphone, tablet, and laptop is about 140 mm × 67 mm × 7.1 mm, 250 mm × 174 mm × 6.1mm and 304 mm × 212 mm × 15 mm, respectively. The simulated and measured results show that the proposed design is a good candidate for cognitive radio applications.

II. Antenna and Circuit Design

A. UWB Antenna Design

Among various monopole patch geometries, the rectangular (30 mm × 50 mm) shaped monopole is initially chosen and optimized to cover 1–5 GHz frequency range. The UWB antenna is designed and optimized in HFSS. 0.7874 mm thick RT/Duroid 5880 substrate with a relative permittivity (ε_r) of 2.2 and loss tangent of 0.0009 is used. The final geometry of the UWB antenna is shown in Fig. 1(a), while the design procedure of the UWB antenna structure is shown in Fig. 1(b). The optimization has been completed with 5 steps as shown in Fig. 1(b). In all the steps, an antenna footprint (substrate size) is not changed. At the first step, a rectangular (30 mm × 50 mm) patch shaped monopole is designed. The monopole antenna is fed at the middle of the bottom edge by 50 ohms feedline. The monopole antenna is separated from the ground plane by 1.97 mm as shown in Fig. 1(a). Based on the current distribution as shown in Fig. 2, a rectangular area of 15 mm × 40 mm is removed to lower the metallic losses at the second step. At the third step, the right side of the patch is truncated by a 10 mm × 10 mm slot, that compensates for the impedance changes due to the inner section removal. As seen in Fig. 1(b), this step improves antenna impedance only for a certain frequency range in the frequency band of interest. As the fourth step,

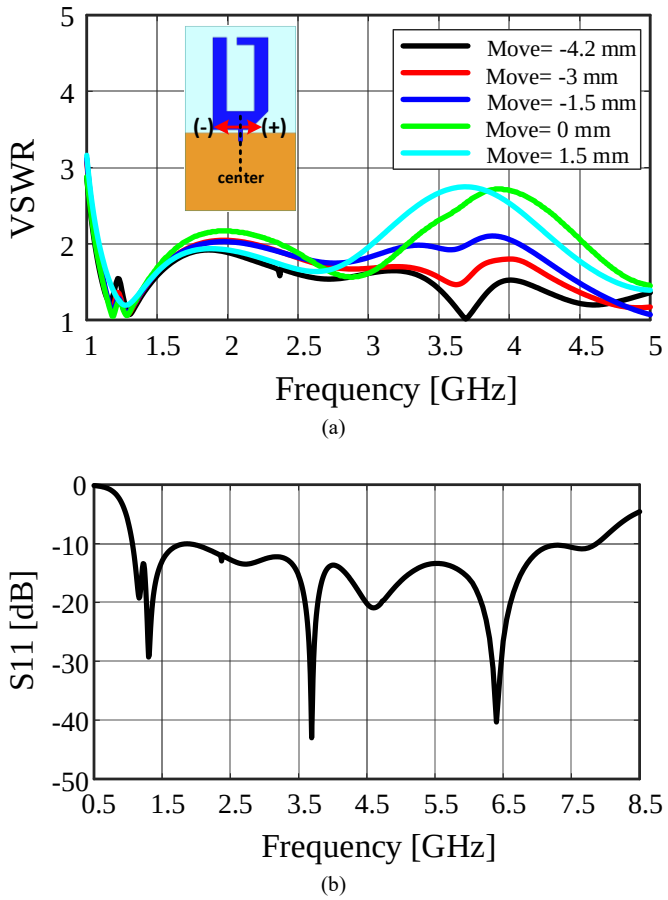

Fig. 3. The finalized UWB antenna: (a) Feed point sweep; (b) Reflection coefficient of finalized UWB antenna

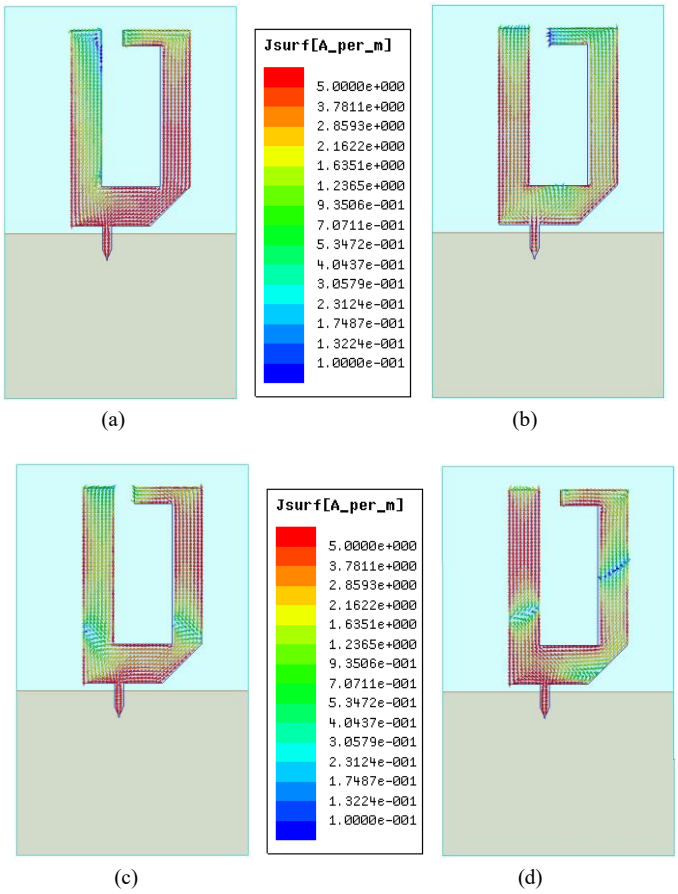

Fig. 4. Surface current distribution of the finalized UWB antenna at various frequencies: (a) 1 GHz; (b) 2 GHz; (c) 3 GHz; (d) 4 GHz

an additional metal strip is added to the truncated side of the antenna to further expand the lower frequency band by elongating the electrical path. Lastly, the feed point is offset from the center in order to find the position that can improve the input impedance at higher frequencies. In Fig. 3(a), the VSWR is shown for different offset locations of the feed line from the center, represented by the parameter, 'Move'. It is observed that the antenna shows a wider bandwidth when the feeding point is moved 4.2 mm away from the center. Fig. 3(b) shows the reflection coefficient of the finalized UWB antenna that covers 1 GHz to 7.85 GHz frequency range.

To illustrate how the antenna works at different frequencies, the surface current distribution was studied. It is observed from Fig. 4(a) and 4(b) that strong current flows on the longer and shorter arms of the antenna at 1 GHz and 2 GHz, respectively. The current concentrates on the right side of the feed at 3 GHz and left side of the feed at 4 GHz as shown in Fig. 4(c) and 4(d), respectively.

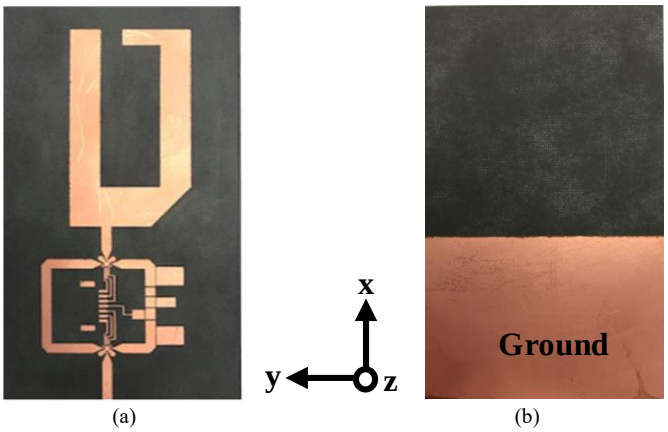

Fig. 5. Fabricated proposed antenna: (a) Top view; (b) Bottom view

B. Matching Circuit Design and Its Operation

The proposed antenna, attached to the matching circuit design as shown in Fig. 5, is fabricated on a 0.7874 mm thick RT/Duroid 5880 substrate with a relative permittivity (ε_r) of 2.2, and loss tangent of 0.0009. Fig. 6(a) shows the working principle of the proposed antenna. The UWB antenna which works from 1–5 GHz frequency range is connected to a discrete switch (PE42422) to create two different paths as shown in Fig. 6(b). An additional switch is used to connect both paths to achieve a single input/output configuration. The first (green)path is used to operate in the 1–5 GHz range and the second (blue) path which goes through a dc-controlled varactor-based matching network is used to operate between 430 MHz and 1 GHz as shown in Fig. 6(c). This unique combination of switches and varactor provides an extremely wide (11.5:1) frequency operation region. The varactor (SMV2203-40LF) based tunable matching network is used

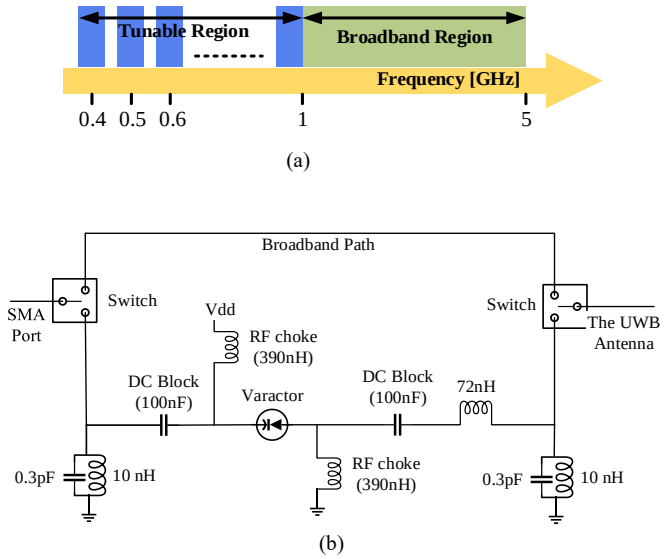

Fig. 6. Operation principle of the proposed antenna: (a) operational diagram; (b) schematic of the reconfigurable section of the antenna; (c) antenna configuration (green arrows show the broadband path and blue arrows show tunable path)

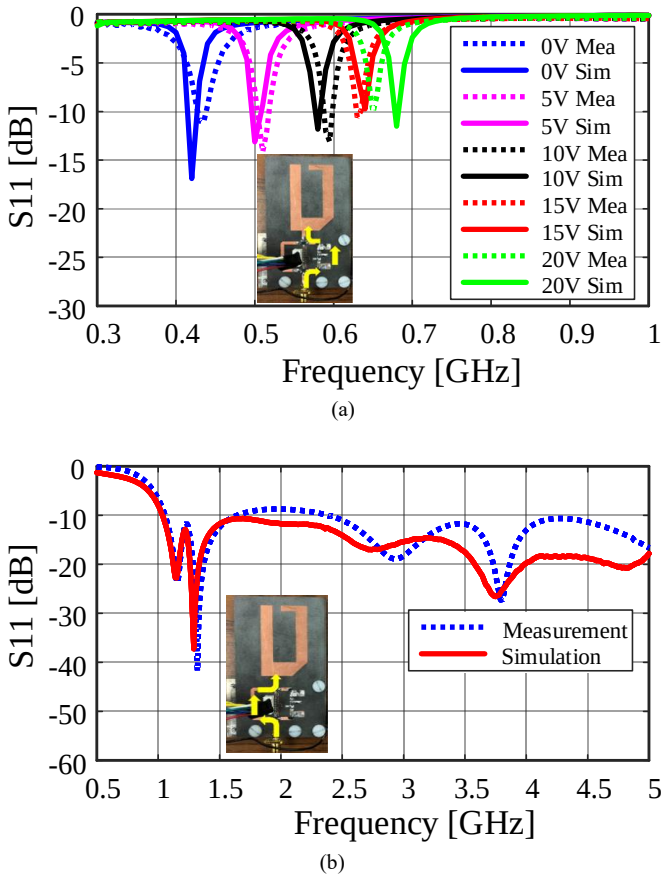

Fig. 7. S_{11} characteristics of the proposed antenna: (a) tunable region; (b) broadband region

TABLE I
COMPARISON OF RECONFIGURABLE UWB ANTENNAS

Ref.	Size (mm^2)	BW (GHz)	BW Ratio	Tuning BW (GHz)	η (%) min/max
[14]	34 × 27	2.7 – 12	4.4:1	0.75	NA
[15]	90 × 50	2.3 – 3.6	1.56:1	1.15	37.2/73.9
[16]	60 × 120	0.75– 7.65	10.2:1	0.74	NA
[30]	38 × 69	1.5 – 4.2	2.8:1	1.8	22/40
[31]	50 × 50	2.10 – 11	5.2:1	3.7	NA
[32]	38.7 × 24.4	2.54 – 10.6	4.2:1	NA	70/80
[33]	24 × 28	3 – 10.5	3.5:1	NA	NA
[34]	65 × 120	0.72 – 3.44	5:01	1.9	10/98
[35]	36 × 40	3.3 – 11	3.33:1	1	70/92
This work	60 × 100	0.43 – 5	11.5:1	0.22	21.3/84

to match the antenna impedance to 50 ohms. By changing the bias voltage of the varactor, operation frequency is swept continuously between 430 MHz and 1 GHz. The varactor biasing circuitry consisted of two RF chokes (390 nH) and DC block caps (100 nF). The RF chokes block the RF signal from both ends of the antenna terminals to the dc power supply and DC block caps isolate the DC current from entering the radiating structure. Both RF chokes and DC block caps have little or no impact on the matching network. Keysight Advanced Design System (ADS) is used to design the matching network.

III. Results and Discussion

Most of the UWB antenna designs in literature are operating above 3 GHz and few of them working below 2 GHz such as [16], [30] and [34]. It is important to point out that most of the reconfigurable UWB antennas in the literature use reconfigurable functionality to reject some existing wireless bands (WLAN, WiMAX, etc.) which operate in the UWB band. However, the antenna proposed in this work uses a tunable matching network to expand its operation of frequency while having a single input/output. Band selection/rejection can be done at other stages in a transceiver chain. The size of the proposed antenna is compact and has a simple planar structure. A comparison of the proposed reconfigurable UWB antenna with some reported in the literature is given in Table I.

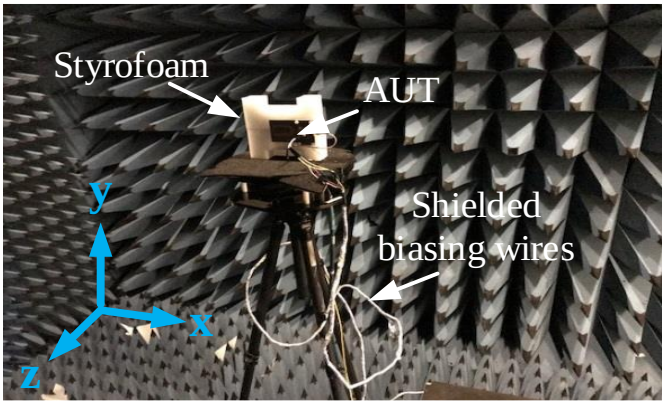

Fig. 8. Far-field radiation pattern (E-plane) measurement setup

A. *Simulated and Measured S-Parameters*

According to the datasheet of the varactor, the tuning range of the varactor diode capacitance is between 4.7 pF and 0.44 pF when the reverse bias voltage is swept from 0 to 20 V. By changing the capacitance of the varactor, the resonance frequency of the UWB antenna is tuned for below 1 GHz. Fig. 7(a) compares simulated and measured reflection coefficients of the tunable region for various biasing voltage of the varactor. Minimum 15 MHz antenna bandwidth (-6 dB BW) is achieved for each reverse biasing voltage. Simulated and measured reflection coefficients for the broadband region are plotted in Fig. 7(b) and -10 dB bandwidth is achieved from 1 GHz to 5 GHz. Discrepancies between the simulated and measured results are attributed to fabrication tolerance and soldering effect.

B. *Far-Field Radiation Characteristics*

The radiation patterns were measured in an anechoic chamber. The dc power supplies were mounted outside of the chamber and aluminum foil shielded wires are used to bias the antenna as shown in Fig. 8. A styrofoam block is used to support the antenna under test.

The measured (co-polarization) and simulated (co and cross-polarization) radiation patterns of the antenna in *xz*-plane (E-plane) and *yz*-plane (H-plane) are presented in Fig. 9. Simulation results show only UWB radiator's radiation properties. However, the measured results include the entire antenna system performance. The small differences between measured and simulated co-polarization radiation patterns are attributed to the antenna fabrication tolerances, possible matching network influences and alignment uncertainties. In general, the antenna radiation patterns are omnidirectional for both tunable and broadband region. Simulated cross-polarization patterns are added for comparison. Cross-polarization patterns are generally below -20dB for both planes. However, some changes are noticed at higher frequencies for both co and cross-polarized patterns, especially at 4 GHz which might be due to the effect of higher-order modes [36].

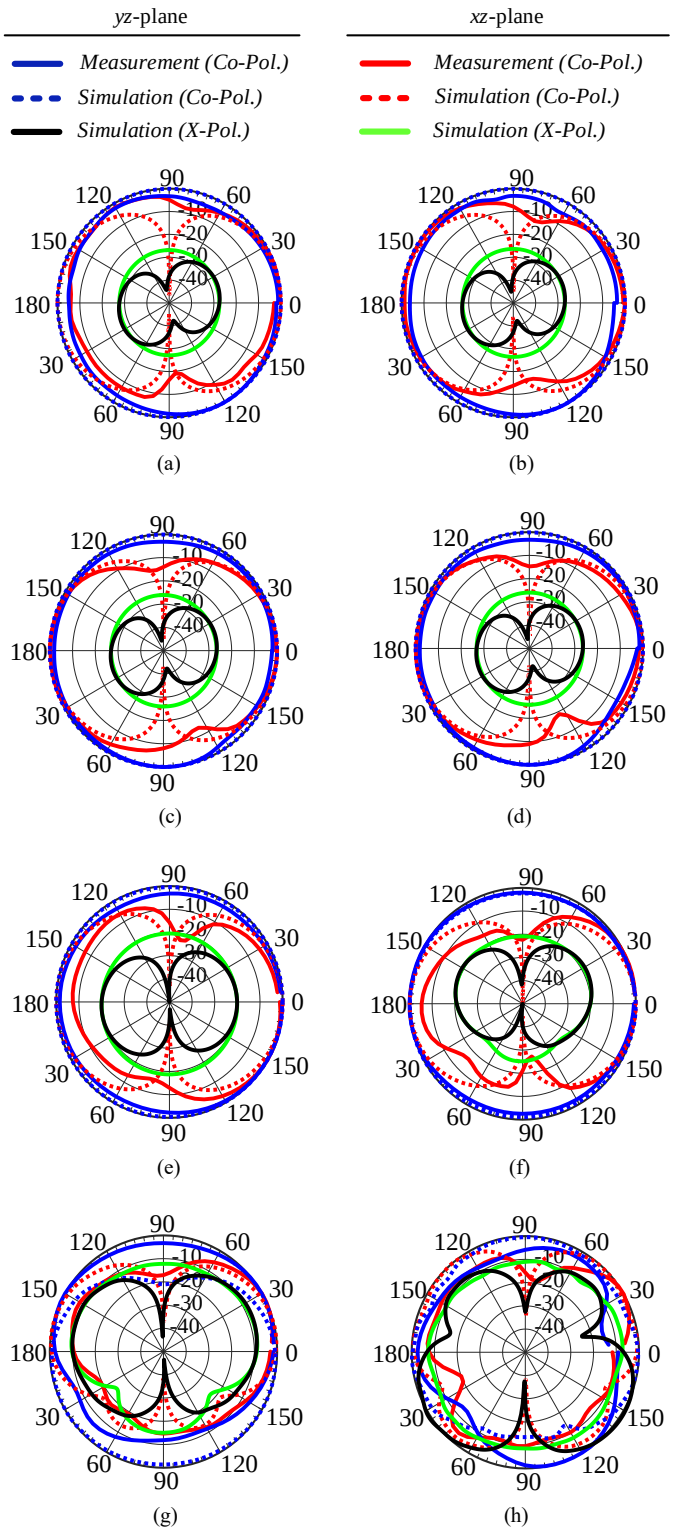

Fig. 9. Measured(co-polarization) and simulated (co and x polarization) normalized radiation patterns at various frequencies: (a) 510 MHz; (b) 595 MHz; (c) 635 MHz; (d) 650 MHz; (e) 1 GHz; (f) 2 GHz; (g) 3 GHz; (h) 4 GHz

C. *Measured Efficiency and Gain*

One of the main disadvantages of using a passive matching network in a reconfigurable antenna is that any losses associated with passive components may reduce overall antenna radiation efficiency. Since the proposed antenna is a reconfigurable electrically small antenna (ESA) below 818MHz, it is important to understand the overall efficiency of the antenna. To compute the efficiency of an antenna with a passive matching network, the antenna is modeled as a 2-port network [37],[38]. A combination of the passive matching network

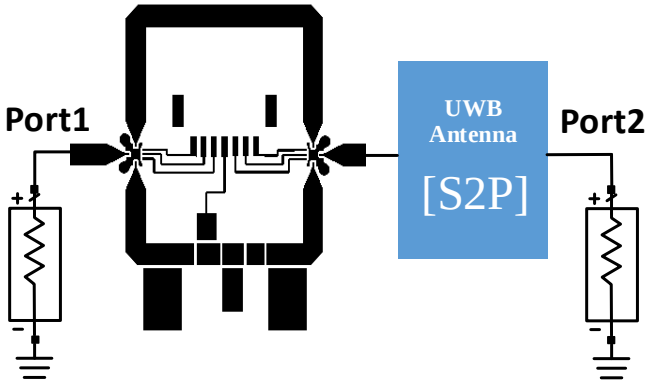

Fig. 10. Schematic for the overall antenna system efficiency calculation

and the two-port model of the antenna can be analyzed by a circuit simulator. Here, we use Keysight Advanced Design Software (ADS)to calculate the overall radiation efficiency. The two-port S-parameters of an antenna is constructed as;

$$[S2P] = \begin{bmatrix} S_{11}^{ant} & S_{21}^{ant} \\ S_{21}^{ant} & S_{11}^{ant} \end{bmatrix} \quad (1)$$

$$|S_{21}^{ant}|^2 = (1 - |S_{11}^{ant}|^2)e_{rad} \quad (2)$$

e_{rad} and S_{11}^{ant} are the radiation efficiency and the antenna reflection coefficient without matching network, respectively. Equation (1) is constructed based on the reciprocity of an antenna (the receive and transmit properties of an antenna are identical). The constructed S2P file is used in ADS as a data file right after the matching network and both ends are terminated with 50-ohms port as shown in Fig.10. The total efficiency(e_{total}) of the entire reconfigurable antenna system is calculated as $|S_{21}^{system}|^2$. The computed overall efficiency of the antenna with a matching network combination is shown in Fig. 11. Tunable region efficiency varies from 20% to 38% at various dc biasing voltages and the broadband region has efficiency above 60%. To verify the predicted results, radiation efficiencies are also measured experimentally using the Wheeler cap technique [39] which is one of the most widely used antenna radiation efficiency measurement techniques because of its simple construction and low cost. A cuboidal wheeler cap is built, and the antenna is placed at the center of the ground plate as shown in Fig. 12(a). In [39] the distance between the antenna and the cap walls is suggested to be $\lambda/2\pi$ and it is assumed that the cap has no effect on current distribution on the antenna. It is also found that the shape of the cap need not be spherical [40]. Three different Wheeler caps are built to measure efficiencies at 450 MHz, 500 MHz, and 600 MHz. Fig. 12(b) shows the measurement setup. Antenna efficiency is calculated by equation (3).

$$e_{rad} = \frac{|S_{11,wc}|^2 - |S_{11,fs}|^2}{1 - |S_{11,fs}|^2} \quad (3)$$

$S_{11,wc}$ and $S_{11,fs}$ are reflection coefficients of the antenna in the Wheeler cap and free space respectively. Simulated and measured

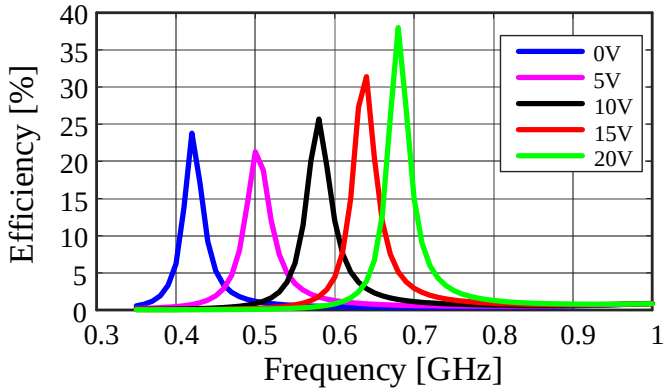

(a)

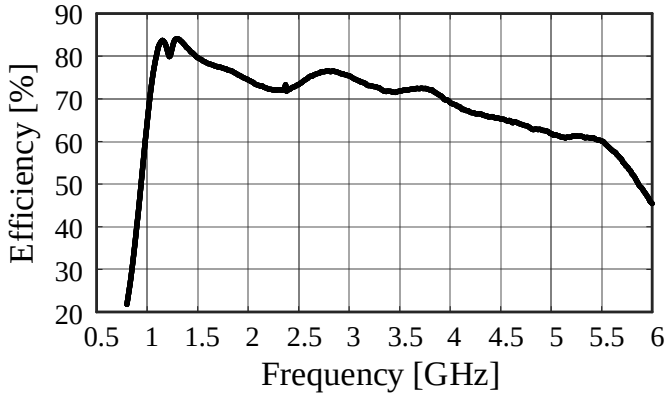

(b)

Fig. 11. Calculated radiation efficiency of the proposed antenna: (a) tunable region efficiencies at various biasing voltage; (b) broadband region efficiency

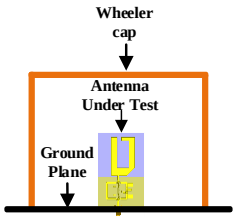

(a)

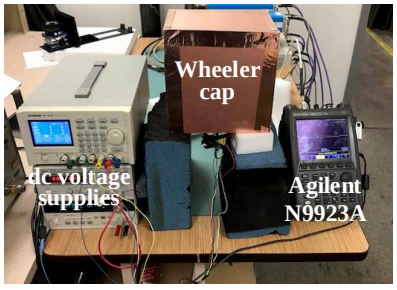

(b)

Fig. 12. Wheeler cap radiation efficiency measurement setup: (a) Schematic View; (b) Experimental view

TABLE II
EFFICIENCY OF THE RECONFIGURABLE UWB ANTENNA

Frequency	Simulation	Measurement
450 MHz	23%	22.1%
500 MHz	22.35%	30%
600 MHz	28%	24%

efficiencies are compared in Table II. Good agreement between the simulation and the measurement is observed.

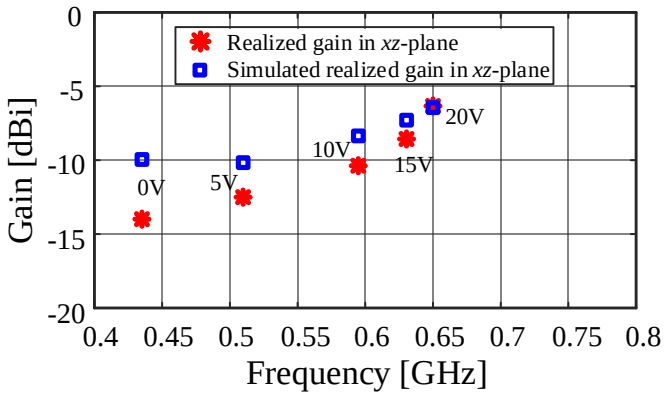

(a)

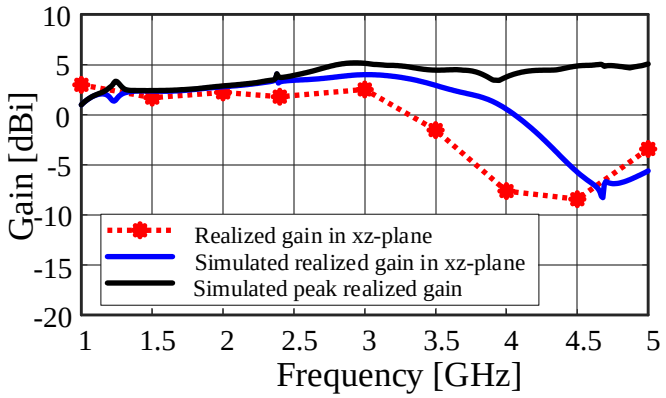

(b)

Fig. 13. Measured gain in the *xz*-plane: (a) tunable region at various biasing voltages; (b) broadband region

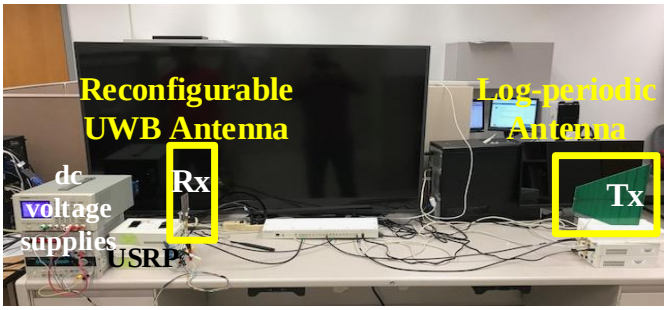

Fig. 14. BER measurement setup

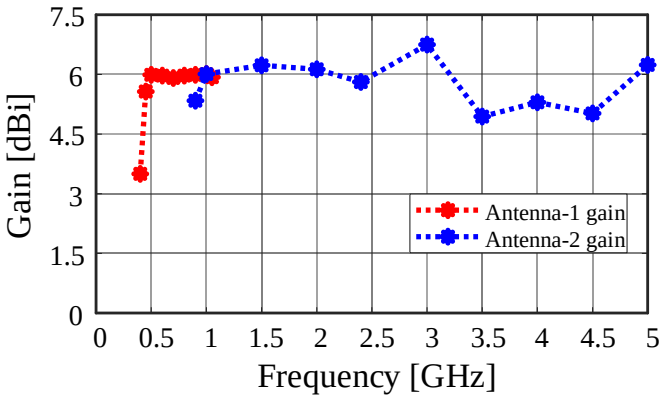

Fig. 15. Log periodic antennas gain (Antenna-1 is used for the tunable region, Antenna-2 is used for the broadband region)

Antenna realized gain is also measured in an anechoic chamber using the Gain-Transfer method in the far field [41]. The measured and simulated realized gains of the reconfigurable UWB antenna in *xz*-plane are plotted in Fig. 13. As mentioned earlier, the antenna can be considered as a reconfigurable ESA below 818 MHz and it is expected to have a gain lower than 0 dBi as reported in [42-45]. Furthermore, it was shown in the literature that antenna ground has an impact on antenna properties such as impedance bandwidth, radiation pattern, and gain. When a cable used to feed an antenna that has an electrically small ground, radiated power decreases due to the current traveling outer surface of the cable [46-49]. In Fig. 13(a), the gain is shown for the tunable region at various biasing voltages. The discrepancy, especially lower frequencies, is likely due to having electrically small ground. Indeed, it is observed that discrepancy gets smaller by frequency. Simulated and measured gains in *xz*-plane are shown in Fig. 13(b) for the broadband region. For comparison, the simulated peak gain of the UWB antenna is depicted in the same figure as well. As mentioned previously, simulation results do not include the impact of the matching network as well as RF switches. Both measured and simulated gain curves follow the same trend and some gain reduction is observed after 3.5 GHz. This reduction in gain can be attributed to the change of radiation pattern with frequency as well as switches' insertion loss. However, it can be observed that the peak gain has a smoother trend with higher gain compared to the one obtained in *xz*-plane and peak gain varies from 1 dBi to 5.1 dBi over the broadband region.

D. Bit Error Rate (BER) Measurement

There are several parameters that affect the performance of the cognitive radio (CR) system which are power/energy, bit error rate (BER), data rate, bandwidth, etc. but out of these BER plays an important role in the performance, capability, and reliability of any communication system. BER is the ratio of how many bits received in error over the number of total bits received. It is affected by many factors such as signal to noise ratio (SNR), distortion and jitter. The CR should be able to detect signals even at very low SNR. The reconfigurable antenna presented here employs several semiconductor elements such as varactor and RF switches. Any noise variation in these elements contributes to the performance of the system; some of such variations cannot be theoretically modeled to examine their effects, but in a real-world data transmission, this may affect the reliability of the communication. Hence, to further evaluate the antenna performance, BER measurement is performed. Single reconfigurable UWB antenna is used for simplicity at the receiver side (Rx) and a log periodic antenna is used at the transmit side (Tx). The reconfigurable UWB antenna is placed 5 feet away from the log periodic antenna as shown in Fig. 14. Both antennas are connected to a Universal Software Radio Peripheral (USRP) and a QPSK modulated signal is used for communication between the Tx and Rx antennas. Gain of the log-periodic antennas that are used in the BER measurement is given in Fig. 15. Antenna-1 and Antenna-2 refer to the antennas that are used in the tunable and broadband region measurements respectively. As mentioned earlier, many factors can affect the BER. In this experiment, the effect of SNR is investigated. To control the SNR value, artificial noise is added to the received

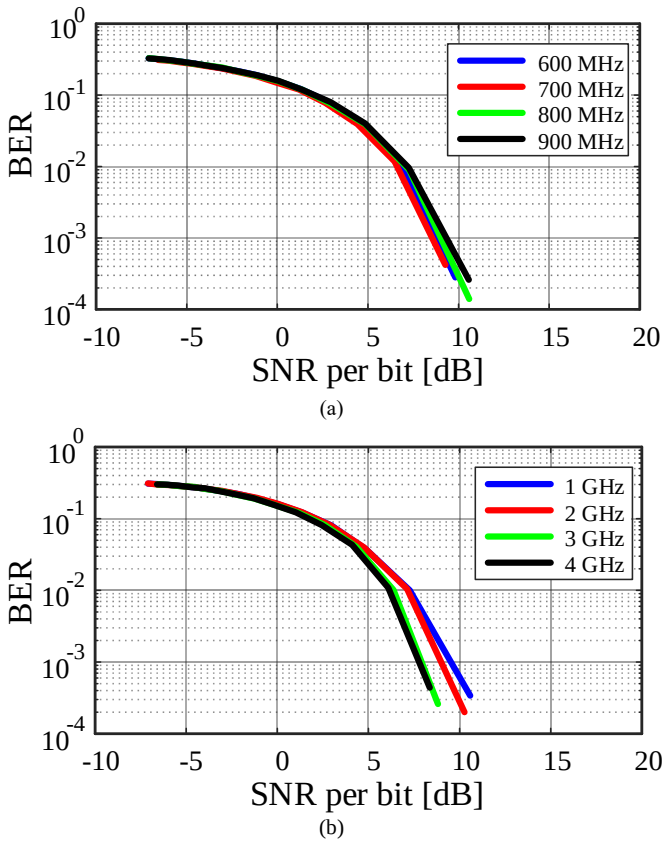

Fig. 16. BER measurement results: (a) tunable region; (b) broadband region

baseband signal. Specifically, once the received SNR is measured and channel estimation and equalization are done by signal processing algorithms at the receiving USRP, artificial noise is added to the I and Q components.

$$SNR_{rec} = \frac{P_{rec}^{norm}}{P_{noise}}(dB) \tag{4}$$

$$SNR_{final} = 10\log[\frac{1}{10^{\frac{-\overline{SNR_{rec}}}{10}} + 2N_{add}^2}](dB) \tag{5}$$

Equation (4) is used to calculate the received SNR denoted by SNR_{rec} and the BER is calculated by comparing the transmitted and received bits. Equation (5) is used to calculate the final SNR. $P_{rec}^{norm}, P_{noise}$ and N_{add} are normalized received power, noise power, and artificial noise respectively. Note that theoretically, there is no need to add artificial noise to the signal to vary the received SNR, as equation (4) readily yields the received SNR value, so varying P_{rec}^{norm} should enable us to control the SNR value. However, varying the value of P_{rec}^{norm} is difficult in practice due to limited granularity in transmit/receive amplifier gains. The process of data transmission is done by sending 500 frames each containing 100 QPSK symbols for a given additive noise value. For each received frame SNR_{rec} is calculated. After receiving the last frame, the average value of SNR_{rec} is also calculated; denoted by $\overline{SNR}_{rec}$. Ultimately, the final value of SNR is calculated using equation (5) and BER is captured. Fig. 16(a) and 16(b) shows the measured BER results for tunable and broadband regions, respectively. It can be observed that the BER curves have a waterfall shape in both operation region**.** According to the Federal Communications Commission (FCC), the minimum detectable received power level should be -114 dBm for coherent signal detection which corresponds to SNR of around -15 dB [50-52], with the BER lower than 0.001. It can be observed from Fig.16 that SNR values are better than 5 dB for 0.001 BER in both the tunable and the broadband region. Hence, the proposed antenna is suitable for cognitive radio applications.

IV. Conclusion

A novel compact reconfigurable UWB antenna is presented. Both discrete switching and continuously tuning techniques are used to obtain large frequency coverage (11.5:1). The measured results show that this antenna can operate from 430 MHz to 5 GHz and has nearly omnidirectional radiation patterns. The realized gain and efficiency of the proposed antenna varies from -14 dBi to 2.98 dBi in *xz*-plane and from 20% to 87%, respectively. SNR values are better than 5 dB for 0.001 BER in both the tunable and broadband region. This work completes every aspect of antenna design for CR communication. The overall results show that the proposed compact reconfigurable UWB antenna is a good candidate for CR platforms, which is a potential solution for overcoming the RF spectrum crowdedness.

References

[1] Ctia.org, “Wireless Snapshot 2017,” 2017. [Online]. Available: https://www.ctia.org/docs/default-source/default-document-library/ctia-wireless-snapshot.pdf.

[2] S. H. Choi, J. K. Park, S. K. Kim, and J. Y. Park, “A New Ultra-wideband Antenna for UWB Applications,” *Microw. Opt. Technol. Lett.*, vol. 40, no. 5,pp.399-401,2004.

[3] J. Liang, C. C. Chiau, X. Chen and C. G. Parini, "Study of a printed circular disc monopole antenna for UWB systems," *IEEE Trans. Antennas Propag.*, vol. 53, no. 11, pp. 3500-3504, Nov. 2005.

[4] C. Y. Huang and W. C. Hsia, “Planar elliptical antenna for ultra-wideband communications,” *IEE Electron. Lett*, vol. 41, no. 6, pp. 296–297, Mar. 2005

[5] J. Kim, T.Yoon, J. Kim and J. Choi, “Design of an ultra wide-band printed monopole antenna using FDTD and genetic algorithm,” *IEEE Microw. Wireless Components Lett.*, vol. 15, no. 6, pp. 395-397, June 2005.

[6] W. J. Krzysztofik, “Modified Sierpinski Fractal Monopole for ISM-Bands Handset Applications,” *IEEE Trans. Antennas Propag.*, vol. 57, no. 3, pp. 606-615, March 2009.

[7] S. Verma and P. Kumar, “Printed Newton's egg curved monopole antenna for ultrawideband applications,” *IET Microw., Antennas & Propag.*, vol. 8, no. 4, pp. 278-286, 18 March 2014.

[8] P. M. Paul, K. Kandasamy, M. S. Sharawi and B. Majumder, “Dispersion-Engineered Transmission Line Loaded Slot Antenna for UWB Applications,” in *IEEE Antennas Wireless Propag. Lett.* vol. 18, no. 2, pp. 323-327, Feb. 2019.

[9] Liang X. L. “Ultra-wideband antenna and design” Ultrawideband-Current Status and Future Trends. London, UK: InTech; 2012.

[10] Allen B., ”Theory of UWB Antenna Elements” Ultra-wideband antennas and propagation for communications, radar and imaging, West Sussex, England: JohnWilley&Sons, 2007, pp 232.

[11] T. Korosec, P. Ritos, and M. Vidmar, “Varactor-tuned microstrip-patch antenna with frequency and polarisation agility,” *Electron. Lett.*, vol. 42, no. 18, pp. 1015-1016, 31 Aug. 2006.

[12] Y. Tawk, J. Costantine, and C. G. Christodoulou, "A Varactor-Based Reconfigurable Filtenna," *IEEE Antennas Wireless Propag. Lett.*, vol. 11, pp. 716-719, 2012.

[13] S.-S. Oh, Y.-B. Jung, Y.-R. Ju, and H.-D. Park, "Frequency-tunable open ring microstrip antenna using varactor," in *Proc. Int. Conf. Electromagn. Adv. Appl*., Sep. 2010, pp. 624–626.

[14] M. Tang, H. Wang, T. Deng, and R. W. Ziolkowski, "Compact Planar Ultrawideband Antennas With Continuously Tunable, Independent Band-Notched Filters," *IEEE Trans. Antennas and Propag*., vol. 64, no. 8, pp. 3292-3301, Aug. 2016.

[15] J. Lim, Z. Jin, C. Song and T. Yun, "Simultaneous Frequency and Isolation Reconfigurable MIMO PIFA Using PIN Diodes," in *IEEE Trans. Antennas Propag.*, vol. 60, no. 12, pp. 5939-5946, Dec. 2012.

[16] R. Hussain, M. S. Sharawi and A. Shamim, "An Integrated Four-Element Slot-Based MIMO and a UWB Sensing Antenna System for CR Platforms," *IEEE Trans. Antennas Propag.*, vol. 66, no. 2, pp. 978-983, Feb. 2018.

[17] P. Qin, Y. J. Guo, A. R. Weily and C. Liang, "A Pattern Reconfigurable U-Slot Antenna and Its Applications in MIMO Systems," *IEEE Trans. Antennas Propag.*, vol. 60, no. 2, pp. 516-528, Feb. 2012.

[18] N. Haider, A. G. Yarovoy and A. G. Roederer, "L/S -Band Frequency Reconfigurable Multiscale Phased Array Antenna with Wide Angle Scanning," *IEEE Trans. Antennas Propag.*, vol. 65, no. 9, pp. 4519-4528, Sept. 2017.

[19] W. H. Weedon, W. J. Payne, and G. M. Rebeiz, "MEMS-switched reconfigurable antennas," *IEEE Antennas Propag.Society Int. Symp*., vol. 3, Jul. 2001, pp. 654–657.

[20] D. E. Anagnostou et al., "Design, fabrication, and measurements of an RF-MEMS-based self-similar reconfigurable antenna," in *IEEE Trans. Antennas Propag.*, vol. 54, no. 2, pp. 422-432, Feb. 2006.

[21] K. R. Boyle and P. G. Steeneken, "A five-band reconfigurable PIFA for mobile phones," in *IEEE Trans. Antennas Propag.*, vol. 55, no. 11, pp. 3300–3309, 2007

[22] G. Lovat, P. Burghignoli and S. Celozzi, "A Tunable Ferroelectric Antenna for Fixed-Frequency Scanning Applications," *IEEE Antennas Wireless Propag. Lett.*, vol. 5, pp. 353-356, 2006.

[23] H. Li, C. Yeh, J. Huang, C. Chang, C. Yu, and J. Fu, "CPW-Fed Frequency-Reconfigurable Slot-Loop Antenna With a Tunable Matching Network Based on Ferroelectric Varactors," *IEEE Antennas Wireless Propag. Lett.*, vol. 14, pp. 614-617, 2015.

[24] L. Tan, R. Wu, C. Wang, and Y. Poo, "Ferrite-Loaded SIW Bowtie Slot Antenna With Broadband Frequency Tunability," *IEEE Antennas Wireless Propag. Lett.*, vol. 13, pp. 325-328, 2014.

[25] F. A. Ghaffar and A. Shamim, "A Ferrite LTCC Based Dual Purpose Helical Antenna Providing Bias for Tunability," *IEEE Antennas Wireless Propag. Lett.*, vol. 14, pp. 831-834, 2015.

[26] A. C. Polycarpou, M. A. Christou, N. C. Papanicolaou, "Tunable patch antenna printed on a biased nematic liquid crystal cell," *IEEE Trans. Antennas Propag.*, vol. 62, no. 10, pp. 4980-4987, Oct. 2014.

[27] Y. Zhao, C. Huang, A. Qing, and X. Luo, "A frequency and pattern reconfigurable antenna array based on liquid crystal technology," *IEEE Photon. J.*, vol. 9, no. 3, Jun. 2017, Art. no. 4600307.

[28] G. Perez-Palomino *et al*., "Design and Experimental Validation of Liquid Crystal-Based Reconfigurable Reflectarray Elements With Improved Bandwidth in F-Band," *IEEE Trans. Antennas and Propag.*, vol. 61, no. 4, pp. 1704-1713, April 2013.

[29] L. Liu and R. J. Langley, "Liquid crystal tunable microstrip patch antenna," *Electron. Lett.*, vol. 44, no. 20, pp. 1179-1180, 25 September 2008.

[30] S. Loizeau and A. Sibille, "Reconfigurable ultra-wide band monopole antenna with a continuously tunable band notch," *IET Microw., Antennas Propag.*, vol. 8, no. 5, pp. 346–350, Apr. 2014.

[31] T. Aboufoul, A. Alomainy, and C. Parini, "Reconfiguring UWB Monopole Antenna for Cognitive Radio Applications Using GaAs FET Switches," *IEEE Antennas Wireless Propag. Lett.*, vol. 11, pp. 392-394, 2012.

[32] Lu, L., Jiao, Y.-C., Wang, R.-Q., Zhang, C. and Qiu, M.-M, "Single-layer differential CPW-FED UWB antenna with common-mode suppressed and band notched applications," *Microw. Opt. Technol. Lett*., 59: 73–77. (2017).

[33] S. M. Abbas, Y. Ranga, A. K. Verma and K. P. Esselle, "A Simple Ultra-Wideband Printed Monopole Antenna With High Band Rejection and Wide Radiation Patterns," *IEEE Trans. Antennas and Propag.*, vol. 62, no. 9, pp. 4816-4820, Sept. 2014.

[34] R. Hussain and M. S. Sharawi, "A Cognitive Radio Reconfigurable MIMO and Sensing Antenna System," *IEEE Antennas Wireless Propag. Lett.*, vol. 14, no. , pp. 257-260, 2015.

[35] E. Erfani, J. Nourinia, C. Ghobadi, M. Niroo-Jazi, and T. A. Denidni, "Design and Implementation of an Integrated UWB/Reconfigurable-Slot Antenna for Cognitive Radio Applications," *IEEE Antennas Wireless Propag. Lett*., vol. 11, pp. 77-80, 2012.

[36] J. Liu, S. Zhong, and K. P. Esselle, "A Printed Elliptical Monopole Antenna With Modified Feeding Structure for Bandwidth Enhancement," in *IEEE Trans. on Antennas and Propag.*, vol. 59, no. 2, pp. 667-670, Feb. 2011.

[37] J. T. Aberle, "Two-Port Representation of an Antenna With Application to Non-Foster Matching Networks," *IEEE Trans. Antennas Propag.*, vol. 56, no. 5, pp. 1218-1222, May 2008.

[38] S. K. Dhar, M. S. Sharawi and F. M. Ghannouchi, "Microwave Connector De-Embedding and Antenna Characterization [Education Corner]," in *IEEE Antennas Propag. Magazine*, vol. 60, no. 3, pp. 110-117, June 2018.

[39] G. Smith, "An analysis of the Wheeler method for measuring the radiating efficiency of antennas," in *IEEE Trans. on Antennas Propag.*, vol. 25, no. 4, pp. 552-556, July 1977.

[40] E. Newman, P. Bohley, and C. Walter, "Two methods for the measurement of antenna efficiency," in *IEEE Trans. on Antennas Propag*., vol. 23, no. 4, pp. 457-461, July 1975.

[41] IEEE Standard Test Procedures for Antennas, in *ANSI/IEEE Std 149-1979* , vol., no., pp.0_1-, 1979.

[42] L. M. Feldner, C. T. Rodenbeck, C. G. Christodoulou, and N. Kinzie, "Electrically Small Frequency-Agile PIFA-as-a-Package for Portable Wireless Devices," *IEEE Trans. Antennas Propag.*, vol. 55, no. 11, pp. 3310-3319, Nov. 2007.

[43] H. Kang and S. Lim, "Electrically Small Dual-Band Reconfigurable Complementary Split-Ring Resonator (CSRR)-Loaded Eighth-Mode Substrate Integrated Waveguide (EMSIW) Antenna," *IEEE Trans. Antennas Propag.*, vol. 62, no. 5, pp. 2368-2373, May 2014.

[44] A. Bakhmutov, N. Knyazev, and V. Chechetkin, "Reconfigurable electrically small split ring resonator antenna," *2017 Int. Applied Computational Electromagn. Society Symp. - Italy (ACES)*, Florence, 2017, pp. 1-2.

[45] Y. Yu, J. Xiong, H. Li and S. He, "An Electrically Small Frequency Reconfigurable Antenna With a Wide Tuning Range," *IEEE Antennas Wireless Propag. Lett*., vol. 10, pp. 103-106, 2011.

[46] Zhi Ning Chen, Ning Yang, Yong-Xin Guo and M. Y. W. Chia, "An investigation into measurement of handset antennas," in *IEEE Trans. on Instrumentation and Measurement*, vol. 54, no. 3, pp. 1100-1110, June 2005.

[47] Y. Zhang and B. Niu, "Compact Ultrawideband (UWB) Slot Antenna with Wideband and High Isolation for MIMO Applications," *Progress In Electromagn. Research C*, Vol. 54, 9-16, 2014.

[48] Y. Lu, Y. Huang, H. T. Chattha and P. Cao, "Reducing Ground-Plane Effects on UWB Monopole Antennas," in *IEEE Antennas and Wireless Propag. Lett*., vol. 10, pp. 147-150, 2011.

[49] Q. Ye, Z. N. Chen and T. S. P. See, "Ground Plane Effect on the Performance of a Butterfly-Shaped UWB Monopole," *2008 International Workshop on Antenna Technology: Small Antennas and Novel Metamaterials*, Chiba, 2008, pp. 334-337.

[50] S. J. Shellhammer, A. K. Sadek and W. Zhang, "Technical challenges for cognitive radio in the TV white space spectrum," *2009 Information Theory and Applications Workshop*, San Diego, CA, 2009, pp. 323-333.

[51] Y. Tang, Q. Zhang and W. Lin, "Artificial Neural Network Based Spectrum Sensing Method for Cognitive Radio," *2010 6th International Conference on Wireless Communications Networking and Mobile Computing (WiCOM)*, Chengdu, 2010, pp. 1-4.

[52] A.Bagwari and G. S. Tomar,"Adaptive double-threshold based energy detector for spectrum sensing in cognitive radio networks", *International Journal of Electronics Letters*, (2013) 1:1, 24-32